Discontinuous Galerkin methods and higher-order temporal approximations for modeling saturated groundwater flow

by

Ian A. Nienhueser

A report submitted to the faculty of the University of North Carolina at Chapel Hill in partial fulfillment of the requirements for the degree of Master of Science in the Department of Environmental Science and Engineering.

Chapel Hill

2002

Approved:

Prof. Cass T. Miller, Advisor

Prof. Michael R. Flynn, Reader

Dr. Matthew W. Farthing, Reader

ABSTRACT

IAN A. NIENHUESER: Discontinuous Galerkin methods and higher-order temporal approximations for modeling saturated groundwater flow
(Under the Direction of Cass T. Miller)

Challenges persist in the accurate and efficient solution of groundwater flow equations for heterogeneous aquifers. Low-order approximations in both space and time have dominated traditional approaches for modeling saturated flow. Comparisons of either a higher-order spatial or temporal approximation with its low-order counterpart have shown significantly improved accuracy and efficiency for higher-order methods. Recently, discontinuous Galerkin methods have been investigated since they readily produce higher-order spatial approximations while still conserving mass locally. Furthermore, they achieve this without requiring the approximation of additional unknowns, such as hydraulic head gradients, as is done with mixed finite element methods. In this work, we apply the discontinuous Galerkin finite element method with an adaptive higher-order time discretization to single-phase groundwater flow in heterogeneous porous media. We compare these results to the standard Bubnov Galerkin finite element method coupled with an adaptive higher-order temporal approximation method on three test problems of varying heterogeneity, while varying spatial and temporal order. We found substantial efficiency and accuracy are achieved by combining two high-order methods in comparison to high-order, low-order and low-order, low-order couplings. We also demonstrated that when coupled with an adaptive higher-order temporal method, discontinuous Galerkin method is capable of high-order L_2 norm h convergence rates as with the non locally mass conservative Bubnov Galerkin method, at a computational expense comparable to that of Bubnov Galerkin.

Notation

Roman Letters

$B^e_{\ell,j}$	value in $[B]$ associated ℓ and j DOFs on element e
$[B]$	stiffness and coupling matrix
$B(\cdot,\cdot)$	stiffness and coupling bilinear operator
f	source function
F	residual function
F_{Ω_e}	mapping function from the reference element to the element e
H^m	Sobolev space
J	jacobian
k_e	spatail order on element e
$\mathbf{k}$	set of all k_e
K	hydraulic conductivity
$\{L\}$	right hand side vector
$L(\cdot)$	right hand side operator
$[M]$	mass matrix
$M(\cdot,\cdot)$	mass bilinear operator
n_i	global norm
n^e_i	local norm
N	number of elements over the domain
P_s	spatial order
P_t	temporal order
P_{k_e}	polynomial subset of H^m of order $\leq k_e$
$P_{\mathbf{k}}$	set of all P_{k_e}
q	mass flux
q_b	q boundary value

s	time step index
S_s	specific storage
t	time
t_0	t initial value
t_{cpu}	CPU time
T	temporal domain limit
u	hydraulic head
$\hat{u}$	u analytic or dense grid solution
$\tilde{u}$	u discrete approximation
u_0	u initial value
u_b	u boundary value
u_ℓ^e	DOF ℓ on element e
v	test function
x	spatial location
x_i	$\Omega_i \cap \Omega_{i+1}$
w	test function
$\mathbf{y}$	DAE dependent variable vector
$\mathbf{y}_0$	$\mathbf{y}$ initial value
$\mathbf{y}'$	$\mathbf{y}$ temporal derivative
$\mathbf{y}'_0$	$\mathbf{y}'$ initial value

Greek Letters

α	FLCBDF coefficient
Γ	boundary of Ω
Γ_D	Dirichlet boundary of Ω
Γ_D^e	$\Gamma_D \cup \Omega_e$
Γ_N	Neumann boundary of Ω
Γ_N^e	$\Gamma_N \cup \Omega_e$
Γ_{int}	set of inter-element boundaries
Γ_{int}^e	$\Gamma_{int} \cup \Omega_e$
ϵ_a	absolute tolerance for DAE integrator
ϵ_{L2}	L_2 error norm

ϵ_r	relative tolerance for DAE integrator
η	total number of DOF
τ_h	partition of Ω
ϕ	basis function
$\hat{\phi}$	basis function on reference element
ϕ_ℓ^e	basis function of order ℓ on element e
Ω	spatial domain
$\hat{\Omega}$	reference element
Ω_e	element e

Abbreviations

BE	backward Euler
BDF	backward difference formula
BG	Bubnov Galerkin
B$G_{P_tP_s}$	Bubnov Galerkin approximation of temporal order P_t and spatail order P_s
CN	Crank-Nicolson
CPU	central processing unit
CV	control volume
DG	discontinuous Galerkin
D$G_{P_tP_s}$	discontinuous Galerkin approximation of temporal order P_t and spatail order P_s
DAE	differential algebraic equation
FD	finite difference
FE	finite element
FEM	finite element method
FLCBDF	fixed leading coefficient backward difference formula
IVP	initial value problem
MFEM	mixed finite element method
MHFEM	mixed hybrid finite element method
MOL	method of lines
ODE	ordinary differential equation
OC	orthogonal collocation

PDE	partial differential equation
SGFE	saturated groundwater flow equation

ACKNOWLEDGMENTS

I would like to take the opportunity to thank my advisor Cass T. Miller for his guidance and encouragement order the last few years.

I would also like to thank Matthew Farthing for his helpful talks and lessons that have taught me a great deal, as well as for his willingness to help me through numerous frustrating bugs.

I would like to thank Michael Flynn for his willingness to join my committee and review my thesis on short notice. I'm sure there is more to come here.

I would like to thank all the other members of Casey's research group for there helpful thoughts, especially Joe Pedit, Chandra Abhishek, Joe Kanney and Doris Pan.

Lastly, I would like to thank my many good friends and family members for the care, support, and enjoyable times they have shared with me, to help get me through this project and others before it.

CONTENTS

LIST OF TABLES

LIST OF FIGURES

Chapter 1

Introduction

Groundwater chemical transport models are used everyday by practitioners and researchers of a wide range of fields to assess and predict effects of aquifer contamination in terms of human health, environmental health and legal obligation. These chemical transport models rely of groundwater flow models, which solve the partial differential equation (PDE) that describes saturated groundwater flow.

Most frequently this equation is solved with low-order temporal approximations combined with either finite difference (FD) or the standard Bubnov Galerkin (BG) finite element method (FEM) in space. The FD method [65, 49, 69, 52] is capable of maintaining a local mass balance and providing a basis to compute accurate pathlines on a structured grid that is irregularly spaced. The standard BG FEM [12, 63, 47, 54] achieves approximations on unstructured irregular grids, allowing it to fit irregular domains naturally. BG FEM also allows for straight forward local refinement of h, gird spacing and p, order, but the results contain discontinuities in the velocity vectors across element faces. These discontinuities result in inaccurate pathlines [28] and elemental mass imbalance [70, 31], while the accuracy of both are essential for chemical transport models [26].

Several methods have been developed to overcome these obstacles. The most

promising include, the mixed finite element method (MFEM) [14, 3, 16, 15, 27, 7, 70, 20, 28, 31, 56] and the discontinuous Galerkin (DG) finite element method [18, 19, 4, 59, 61, 62, 4, 6, 41]. Both of these methods achieve local mass balance and accurate path lines on an irregular grid. To accomplish this, the MFEM requires the solution of flux as a variable in addition to the usual hydraulic head, while DG does not [58]. In addition DG is capable of high-order convergence rates and is well suited for adaption [58].

Research has shown substantial improvements in accuracy and efficiency can be achieved by using higher-order solution methods in either space or time in comparison to low-order methods when coupled with low-order methods in the remaining dimension [52, 31, 62]. Further improvements have been found by using higher-order methods in both space and time [24, 60].

This study serves as a preliminary analysis of the benefits achieved by combining the higher-order DG spatial method with higher-order adaptive BDF in time. To our knowledge this study represents a first for this coupling. We will also draw comparisons to adaptive BDF's with standard BG FEM. For our DG method we chose the well suited formulation by Oden, Babuska, et al in [58].

Chapter 2

Background

2.1 Model Formulation

The saturated groundwater flow equation (SGFE) is the partial differential equation that results from the substitution of Darcy's law into a simple mass balance equation. Through laboratory experiments Henry Darcy found the empirical relationship that the volumetric rate of flow through a sand column was proportional to the area of the column and the loss in hydraulic head across the column and inversely proportional to the length of the column in [25].

Hydraulic conductivity is the proportionality coefficient in Darcy's law. SGFE also requires specific storage as a parameter to account for the elasticity of the porous medium under hydraulic pressure. The values of both these parameters can be determined through laboratory experiments or by one of a number of mathematical approximations.

The SGFE is well established. It is routinely used to accomplish successful groundwater flow modeling [36]. However, challenges persist in field scale parameter determination and in the development of accurate and efficient numerical solution methods.

2.2 Spatial Discretization

Spatial methods of approximation that have been used to solve the elliptic and parabolic equations such as SGFE include FD, orthogonal collocation (OC), OC on finite elements (FE), BG FEM, MFEM and DG FEM.

The FD method produces approximations on a structured grid with irregular spacing. The resulting solution displays accurate velocity fields and local mass balance. FD was used extensively in 1978 by Crittenden and Weber in there models of fixed bed adsorbers [67, 22, 23, 21]. Due to its mass conservation and ease of implementation FD is still used in the majority of saturated flow modeling done today, as it is the basis of the popular MODFLOW package. For these reasons as well as grid spacing adaptability and the lack of need for higher-order with non-smooth solutions, FD is still at the leading edge of unsaturated flow research [52].

Villadsen and Stewert developed OC in 1967 [66]. OC is a special case of the method of weighted residuals developed by Finlayson in 1972 [33] and is capable of producing high-order approximations to the solution of PDE's on a structured regular grid. It was applied to the elliptic terms of packed bed analysis by Finlayson [34] in 1971 and by Crittenden in 1980 [24]. OC was extended to OC on FE by Carey and Finlayson in 1975 [11] and by Chang and Finlayson to OC on FE for elliptic equations in [13]. OC on FE allows for variable grid spacing at high-orders. Carey and Finlayson noted similar results to those of FEM.

FEM was developed independently and in parallel by a number of researchers of various fields. Douglas developed a mathematical foundation for the FEM in 1972 [46]. FEM has been and continues to be used in a wide array of fields ranging from flow modeling to structural engineering. Over the years FEM has become a large class of methods that continues to grow. Those most applied to groundwater flow include BG FEM, control volume (CV) FEM, MFEM and DG

FEM. BG is capable of high-order convergence rates on unstructured variable grids with PDE parameters that vary continuously over the domain or discretely between elements. However, as noted earlier, the application of BG to groundwater flow results in elemental mass imbalance [70, 31] and inaccurate velocity fields, [28] while precise mass balance and velocity fields are required for accurate contaminant transport modeling [26]. Attempts to overcome these shortcomings has resulted in CV FEM [35, 69], MFEM [14, 3, 16, 15, 27, 7, 70], DG FEM [18, 19, 4, 59, 61, 62, 4, 6, 41] and the post-processing of pressure fields obtained by BG [20, 28]. MFEM has been found to have advantages over the CV FEM [28] and BG [57, 43].

MFEM is a collection of methods that overcome these mass balance errors by enforcing mass balance across element boundaries through the solution of flux in addition to the usual hydraulic head. However, the standard MFEM produces a symmetric, indefinite linear system that can be poorly conditioned and as a result, difficult to solve [42, 10, 8]. The mixed hybrid FEM (MHFEM) results in a positive definite linear system through the use of additional Lagrange multipliers, which represent the average pressure on the element face [10, 14]. MHFEM is capable of producing second-order convergence rates on irregular unstructured grids, while maintaining local mass balance and an accurate flow field. Because of these abilities, MFEMs continues to be researched within the groundwater field for both saturated [14, 29, 2, 45, 14, 1, 17, 71, 31] and unsaturated [3, 16, 15, 27, 8, 44, 56] flow.

The DG method includes a class of FEMs sharing the commonality of Legendre polynomial basis functions that are discontinuous between elements. DG has been used to solve a number of hyperbolic [18, 19, 4] as well as elliptic and parabolic [59, 61, 62, 4, 6, 41] problems. Oden, Babuska, et al developed the DG method for diffusion problems in 1998 [58], based on the formulations of Wheeler in 1978 [68]. This method can deliver high-order accuracy, exhibits local mass conservation and is well suited for adaption. Two papers have covered the ap-

plication of DG to saturated groundwater flow simulation [62, 6]. Both achieve local mass balance and high-order convergence rates and are based on the DG formulations found in [58, 5]. Riviere and Wheeler [62] demonstrate solutions based on continuous and discontinuous parameterizations in two and three spatial dimensions, while Bastian and Reichenberger [6] present a multigrid method applied to the DG method in two dimensions. DG is an active area of research.

2.3 Temporal Discretizations

In 1969 Gear developed a method for the automated integration of stiff ordinary differential equation (ODE's) in [37], an extension of his earlier work in 1967 [38]. This method is capable of sixth-order convergence rates. When the differential-algebraic equations (DAE) resulting from the application of the MOL coupling method are converted to ODE's they often lose their algebraic constraints, become more stiff and/or lose their sparseness, obviously decreasing their viability and adding to the computational expense of solution [9, 53, 64]. As a result directly solving this DAE system is often more accurate and efficient.

In 1971 Gear produced the BDF method for the solution of DAE [39], which remains the basis for many of the DAE solvers of today. The BDF discretizes the temporal domain of DAE systems with the use of Lagrange polynomials. This integration produces an algebraic system that can be solved by one of the publicly available solvers. Adaptive DAE solvers can produce high-order approximations to a level of accuracy determined by user provided error tolerances [50]. There are many efficient DAE solvers currently available, while this continues as an active area of research [9].

2.4 Coupling

The MOL has been used extensively as a coupling mechanism for more than 20 years [24, 60, 51, 30, 32]. It allows for PDE systems to be converted to systems of DAEs by maintaining a continuous temporal domain and discretizing the spatial domain with the use of a spatial discretization method. The temporal domain is maintained in a continuous fashion through a variable representation of the temporal solution derivative. The temporal domain of the resulting DAE system is then discretized [50].

After Crittenden and Weber's extensive work with the use of low-order FD coupled with second-order CN in the modeling of adsorbate concentrations in the effluent of fixed-bed granular activated carbon reactors [67, 22, 21, 23] and similar models by Finlayson with OC in 1971 [34], Crittenden, Wong, et al combined high-order OC [66] with Gear's sixth-order solver for stiff ODE's [37] in 1980 [24], through this use of the MOL. While high-order in both space and time, this model was limited to one spatial dimension, as well as to a spatial grid and PDE parameters that were uniform throughout the domain.

In 1988 Pedit and Miller combined BG FEM with Gear's ODE solver [40] to examine the effect of varying spatial order between one and twelve on a fixed number of nodes [60]. They modeled the competitive sorption of solutes on solids in a completely mixed batch reactor in the radial spatial dimension of the spherical coordinate system. There findings showed that with high-order in time, error can be reduced by increasing spatial order.

Kees and Miller combined their adaptive high-order MOL DAE solver [50] with FD to solve Richards' equation and the two-phase flow equation in one spatial dimension while analyzing several model formulations for there mass conservation abilities in 2002 [51]. This study showed that the temporally adaptive high-order integration method provide substantial efficiency improvements over first-order methods for a wide range of parameterizations, while maintaining an

accurate local mass balance with the mass-pressure form of Richards equation and the saturation-pressure form of the two phase flow equation.

Farthing, Kees, et al coupled the mass conservative three-dimensional low-order MHFEM with the same MOL DAE solver to solve the SGFE and conducted comparisons to CN and adaptive CN in 2002 [30]. They found this to be a generally successful coupling without excessive overhead and that computational savings were gained by using the DAE solver over the use of CN and adaptive CN.

In 2002 Farthing, Kees, et al successfully solved the pressure form and a mass conservative form of Richards' equation by coupling MHFEM and the enhanced cell-centered difference MFEM with Kees's MOL DAE solver in two spatial dimensions, while comparing temporal orders [32]. The adaptive high-order temporal method showed to be more efficient than adaptive first-order for all cases tested, even when then spatial discretization dominated the computational expense.

As a whole, these and other studies show that substantial improvements in computational expense and accuracy are gained across a wide array of problems by increasing order in space or time or both.

Chapter 3

Approach

3.1 Introduction

We have combined the DG method in space with an adaptive higher-order MOL in time to solve the time dependent SGFE in one spatial dimension. This chapter covers a description of the problem formulation, spatial approximation, temporal approximation, linear system solution methods, a high level algorithm, and other implementation details.

3.2 Problem Formulation

The one dimensional SGFE solved in this study stems from the substitution of Darcy's law into a simple mass balance equation, where through the application of a representative elementary control volume, mass is replaced by such a volume multiplied by media porosity and fluid density, while making appropriate assumptions. Slightly compressible flow has been assumed, meaning the spatial derivative of the fluid density is insignificant relative to its temporal derivative. We have also assumed that the temporal temperature fluctuation and chemical constituent concentration are small and thus have an insignificant effect on the

fluid density. Under these conditions the SGFE takes the form

$$S_s \frac{\partial u}{\partial t} = -\frac{\partial q}{\partial x} + f \qquad \text{in } \Omega \times [0, T] \tag{3.1}$$

with

$$q = -K \frac{\partial u}{\partial x} \tag{3.2}$$

where q is fluid mass flux, u is hydraulic head, K is hydraulic conductivity, S_S is specific storage accounting for the compressibility on the fluid and media under pressure, f is a source function, $\Omega \subset \Re^1$ is the spatial domain and [0,T] is the temporal domain. Further detail on this derivation is available in groundwater textbooks, including [36].

The initial and boundary conditions considered include

$$u(x \in \Omega, t = 0) = u_0 \tag{3.3}$$

$$u(x \in \Gamma_D, t \in [0, T]) = u_b \tag{3.4}$$

$$q(x \in \Gamma_N, t \in [0, T]) = q_b \tag{3.5}$$

where u_0 is an initial condition function, u_b and q_b are boundary condition functions, Γ is the boundary of Ω, $\Gamma_D \cup \Gamma_N = \{x_1, x_N\}$ and $\emptyset = \Gamma_D \cap \Gamma_N$.

3.3 Spatial Approximation

3.3.1 Variational Formula Derivation

Following from [6, 58, 5], let τ_h be a partition of Ω into N elements $\Omega_e = (x_e, x_{e+1})$. $\mathbf{n}_i$ is a unit outward vector on $\{x_1, x_N\}$ that is also arbitrarily chosen to point toward the element with lower index on interior points Γ_{int} located at the element edges.

The DG method approximates weak solutions in finite-dimensional subspaces of the broken Sobolev space

$$H^m(\tau_h) = \{v \in L^2(\Omega) : v|_{\Omega_e} \in H^m(\Omega_e) \forall \Omega_e \in \tau_h\} \tag{3.6}$$

where $m \geq 1$. So the functions may be discontinuous at element boundaries.

It is also useful to define inter-element jumps and averages of a function $v \in H^m(\tau_h)$ as,

$$[v](x_i) = v(x_i)|_{\Omega_e} - v(x_i)|_{\Omega_f}, \qquad e > f, \qquad x_i = \Omega_e \cap \Omega_f, \tag{3.7}$$

and

$$\langle v \rangle(x_i) = \frac{n_i}{2}(v(x_i)|_{\Omega_e} + v(x_i)|_{\Omega_f}), \qquad x_i = \Omega_e \cap \Omega_f, \tag{3.8}$$

From these definitions, for functions $v, w \in H^m(\tau_h)$, we can see the identity

$$[vw](x_i) = ([v]\langle w \rangle + \langle v \rangle [w])(x_i), \tag{3.9}$$

Starting from the SGFE 3.1, for $v \in H^m(\tau_h)$ we have,

$$\int_\Omega v \frac{\partial q}{\partial x} dx + \int_\Omega v S_s \frac{\partial u}{\partial t} dx = \int_\Omega v f dx. \tag{3.10}$$

Breaking this integration into a sum of elemental integrations,

$$\sum_{\Omega_e \in \tau_h} \int_{\Omega_e} v \frac{\partial q}{\partial x} dx + \sum_{\Omega_e \in \tau_h} \int_{\Omega_e} v S_s \frac{\partial u}{\partial t} dx = \sum_{\Omega_e \in \tau_h} \int_{\Omega_e} v f dx. \tag{3.11}$$

Applying Green's theorem,

$$\begin{aligned} -\sum_{\Omega_e \in \tau_h} \int_{\Omega_e} q \frac{\partial v}{\partial x} dx + \sum_{\Omega_e \in \tau_h} \{(vq)(x_{e+1})|_{\Omega_e} - (vq)(x_e)|_{\Omega_e}\} \\ + \sum_{\Omega_e \in \tau_h} \int_{\Omega_e} v S_s \frac{\partial u}{\partial t} dx = \sum_{\Omega_e \in \tau_h} \int_{\Omega_e} v f dx. \end{aligned} \tag{3.12}$$

Noting that,

$$\begin{aligned} &\sum_{\Omega_e \in \tau_h} \{(vq)(x_{e+1})|_{\Omega_e} - (vq)(x_e)|_{\Omega_e}\} \\ &= \sum_{x_i \in \Gamma_{int}} [vqn_i](x_i) + \sum_{x_i \in \Gamma_D} (vqn_i)(x_i) + \sum_{x_i \in \Gamma_N} (vq_b)(x_i), \end{aligned} \tag{3.13}$$

where

$$[vqn_i](x_i) = ([v]\langle qn_i\rangle + \langle v\rangle[qn_i])(x_i), \tag{3.14}$$

while $(\langle v\rangle[qn_i])(x_i)$ is the flux jump between to elements, which if q is the solution, must be zero. So,

$$[vqn_i](x_i) = ([v]\langle qn_i\rangle)(x_i). \tag{3.15}$$

Substituting Darcy's law 3.2 into our weak formulation 3.12, while applying 3.13 and 3.15 we get,

$$\sum_{\Omega_e\in\tau_h}\int_{\Omega_e} K\frac{\partial u}{\partial x}\frac{\partial v}{\partial x}dx - \sum_{x_i\in\Gamma_{int}}\left([v]\left\langle K\frac{\partial u}{\partial x}n_i\right\rangle\right)(x_i) - \sum_{x_i\in\Gamma_D}\left(vK\frac{\partial u}{\partial x}n_i\right)(x_i) \tag{3.16}$$
$$+\sum_{x_i\in\Gamma_N}(vq_b)(x_i), + \sum_{\Omega_e\in\tau_h}\int_{\Omega_e} vS_s\frac{\partial u}{\partial t}dx = \sum_{\Omega_e\in\tau_h}\int_{\Omega_e} vf dx.$$

The weak continuity of the solution at element boundaries requires that

$$\sum_{x_i\in\Gamma_{int}}\left(\left\langle K\frac{\partial v}{\partial x}n_i\right\rangle[u]\right)(x_i) = 0 \tag{3.17}$$

and

$$\sum_{x_i\in\Gamma_D}\left(K\frac{\partial v}{\partial x}n_i\right)(u-u_b)(x_i) = 0. \tag{3.18}$$

These requirements are added as penalty terms to the weak formulation 3.16, which when restructured becomes:

$$\text{find } u\in H^m(\tau_h) \qquad \text{such that} \qquad B(v,u)+M\left(v,\frac{\partial u}{\partial t}\right) = L(v), \qquad \forall v\in H^m(\tau_h), \tag{3.19}$$

where

$$B(v,u) = \sum_{\Omega_e\in\tau_h}\int_{\Omega_e} K\frac{\partial u}{\partial x}\frac{\partial v}{\partial x}dx \tag{3.20}$$
$$+\sum_{x_i\in\Gamma_{int}}\left(\left\langle K\frac{\partial v}{\partial x}n_i\right\rangle[u] - [v]\left\langle K\frac{\partial u}{\partial x}n_i\right\rangle\right)(x_i),$$
$$+\sum_{x_i\in\Gamma_D}\left(K\frac{\partial v}{\partial x}n_i u - vK\frac{\partial u}{\partial x}n_i\right)(x_i)$$

$$M\left(v, \frac{\partial u}{\partial t}\right) = \sum_{\Omega_e \in \tau_h} \int_{\Omega_e} S_s v \frac{\partial u}{\partial t} dx, \tag{3.21}$$

$$L(v) = \sum_{\Omega_e \in \tau_h} \int_{\Omega_e} v f dx + \sum_{x_i \in \Gamma_D} \left(K \frac{\partial v}{\partial x} n_i u_b\right)(x_i) - \sum_{x_i \in \Gamma_N} (v q_b)(x_i), \tag{3.22}$$

The same steps of derivation can also be applied to the initial condition to obtain,

$$u_e(0) = \sum_{\Omega_e \in \tau_h} \int_{\Omega_e} u_0 v dx. \tag{3.23}$$

3.3.2 Discrete Formula Derivation

In the discrete formulation, the Sobolev space $H^m(\Omega_e)$ is replaced by $P_{k_e}(\Omega_e) \subset H^m(\Omega_e)$, consisting of polynomials of degree k_e on Ω_e. Stability of the method was proven for $k_e >= 2$ by Oden, Babuska, et al [58]. These polynomials are produced through the mapping of polynomials on a reference element,

$$P_{k_e}(\Omega_e) \quad = \quad \left\{\phi \mid \phi = \hat{\phi} \circ F_{\Omega_e}^{-1}, \hat{\phi} \in P_{k_e}(\hat{\Omega})\right\} \tag{3.24}$$

where $F_{\Omega_e} : \hat{\Omega} \rightarrow \Omega_e$ is a mapping from the reference element to the element Ω_e. We chose to let $P_{k_e}(\Omega_e)$ be the set of, the commonly used, Legendre polynomials up to order k_e. Our discrete solution space becomes,

$$P_{\mathbf{k}}(\tau_h) = \prod_{\Omega_e \in \tau_h} P_{k_e}(\Omega_e) \tag{3.25}$$

where vector $\mathbf{k}$ consists of elements k_e. Let

$$\eta = \text{Card} P_{\mathbf{k}}(\tau_h). \tag{3.26}$$

From the variational formula the discrete formulation used in this work is obtained by letting

$$v = \sum_{\Omega_e \in \tau_h} \sum_{\ell=0}^{k_e} \phi_\ell^e(x) \tag{3.27}$$

and by replacing u with ũ,

$$\tilde{u} = \sum_{\Omega_e \in \tau_h} \sum_{j=0}^{k_e} u_j^e(t) \phi_j^e(x) \tag{3.28}$$

with ϕ_ℓ^e and $\phi_j^e \in P_{k_e}(\Omega_e)$, where $k_e + 1$ is the number of degrees of freedom (DOF) u_j^e on Ω_e. It is also useful to recognize that

$$\left\langle K\frac{\partial \phi_\ell^e}{\partial x}n_i \right\rangle = K\frac{n_i}{2}\frac{d\phi_\ell^e}{dx}(x_i)|_{\Omega e} \tag{3.29}$$

and

$$[\phi_\ell^e](x_i) = n_i n_i^e \phi_\ell^e(x_i)|_{\Omega e}, \tag{3.30}$$

where n_i^e is the outward unit normal to the end point x_i of Ω_e. With these substitutions and simplification the discrete formulation becomes

$$\begin{aligned} \text{find } u_j^e \text{ such that } B(\phi_\ell^e, \phi_j^e)\{u_j^e\} + M(\phi_\ell^e, \phi_j^e)\left\{\frac{du_j^e}{dt}\right\} = L(\phi_\ell^e), \\ \forall \phi_\ell^e \text{ and } \phi_j^e \in P_{\mathbf{k}}(\tau_h), \end{aligned} \tag{3.31}$$

where

$$\begin{aligned} B(\phi_\ell^e, \phi_j^e) = \int_{\Omega_e} K\frac{d\phi_\ell^e}{dx}\frac{d\phi_j^e}{dx}dx + \sum_{x_i \in \Gamma_D^e} Kn_i\left(\frac{d\phi_\ell^e}{dx}\phi_j^e - \phi_\ell^e\frac{d\phi_j^e}{dx}\right)(x_i) \\ + \sum_{x_i \in \Gamma_{int}^e} K\frac{n_i n_i^e}{2}\left(\frac{d\phi_\ell^e}{dx}\phi_j^e - \phi_\ell^e\frac{d\phi_j^e}{dx}\right)(x_i), \end{aligned} \tag{3.32}$$

$$M(\phi_\ell^e, \phi_j^e) = -\int_{\Omega_e} S_s \phi_\ell^e \phi_j^e dx, \tag{3.33}$$

$$L(\phi_\ell^e) = -\int_{\Omega_e} f\phi_\ell^e dx + \sum_{x_i \in \Gamma_D^e} Kn_i u_b \frac{d\phi_\ell^e}{dx}(x_i) + \sum_{x_i \in \Gamma_N^e} q_b \phi_\ell^e(x_i), \tag{3.34}$$

and the initial DOF are obtained by

$$u_\ell^e(0) = \frac{2\ell + 1}{2}\int_{\Omega_e} u_0 \phi_\ell^e dx \tag{3.35}$$

$\Gamma_D^e = \Gamma_D \cup \Omega_e$, $\Gamma_N^e = \Gamma_N \cup \Omega_e$ and $\Gamma_{int}^e = \Gamma_{int} \cup \Omega_e$.

3.4 Temporal Approximation

We used an adaptive fixed leading coefficient backward difference formula (FLCBDF) MOL for time integration [50]. This section will cover the aspects of

this method that pertain to its implementation with DG. Further details on this method are available in the literature [9, 50, 48].

Implementation of this solver requires providing a description of the initial value problem (IVP) to be solved. This description includes the DAE system, initial values and an optional Jacobian. In the most general case this DAE takes the form of the nonlinear fully implicit vector function

$$F(t, \mathbf{y}, \mathbf{y}') = 0 \tag{3.36}$$

where $t \in \Re^1, \mathbf{y}, \mathbf{y}' \in \Re^\eta$, and $F : \Re^{2\eta+1} \rightarrow \Re^\eta$. In the case of the solution sought in this study F, commonly called the residual function, takes the form

$$F\left(t, \{u_j^e\}, \left\{\frac{du_j^e}{dt}\right\}\right) = [B]\{u_j^e\} + [M]\left\{\frac{du_j^e}{dt}\right\} - \{L\} = 0 \tag{3.37}$$

where $[B]$ consists of values $B_{\ell,j}^e$, which result from the global application of the bilinear $B(\phi_\ell^e, \phi_j^e)$ such that $B_{\ell,j}^e = B(\phi_\ell^e, \phi_j^e)\ \forall \phi_\ell^e, \phi_j^e \in P_{\mathbf{k}}(\tau_h)$ and likewise for $[M]$ and $\{L\}$. The initial values required include t_0, $\mathbf{y_0}$ and $\mathbf{y'_0}$. For our study $\mathbf{y_0} = \{u_j^e(0)\}$. Approximate values are sufficient for $\mathbf{y'_0}$, which we set to the elementwise division of $\{b\}$ by $\{m\}$ where

$$\{b_j^e\} = -[B]\{u_j^e\} + \{L\} \tag{3.38}$$

and $\{m\}$ holds the row summations of $[M]$. Generally, with time t_s at the temporal step s, the Jacobian

$$[J_s] = \alpha_s \left[\frac{\partial F_s}{\partial y'}\right] + \left[\frac{\partial F_s}{\partial y}\right] \tag{3.39}$$

where

$$\alpha_s = \frac{1}{t_s - t_{s-1}} \sum_{j=1}^{k_t} \frac{1}{j} \tag{3.40}$$

and k_t is the order of the temporal approximation. In the case of the linear system solved in this study, the Jacobian simply becomes

$$[J_s] = \alpha_s[M] + [B]. \tag{3.41}$$

With this IVP the DAE solver can produce the solution and its first temporal derivative at a finite number of times on the interval $[t_0, T]$.

These values are obtained by taking time steps as described by this algorithm [50]:

1. form an explicit prediction to the solution of the DAE by extrapolating from the solution history, with a Lagrange polynomial of suitable order

2. form a corrector equation for the unknown solution vector y_{n+1} using a Lagrange polynomial of suitable order that terminates at the unknown solution point

3. if possible, define the value of the corrector equation by algebraically solving it, requiring that it satisfy Equation 3.36 to an appropriate error tolerance, otherwise reduce step-size and/or order and retry the step

4. update the solution history

5. estimate the allowable step-size and order of the solution method for the next step

6. output solution information if desired after performing any necessary interpolation

The user can control the temporal error of this solution method by setting the absolute and relative tolerances represented by ϵ_a and ϵ_r. Guidelines for setting these values are setting ϵ_a to a solution value that is considered insignificant and setting $\epsilon_r = 10^{-m-1}$ for m significant digits of the solution $\tilde{u}$ [9]. Since most the computation required by this method is spent solving the algebraic systems produced, the choice of solution method for these systems greatly effects the performance of the DAE solver.

3.5 Linear System Solution Method

Since the PDE we are solving is linear, the algebraic system solved in step 3 of the DAE algorithm discussed in Section 3.4 is a linear system. With the application of DG in one spatial dimension, this linear system has an asymmetric block-diagonal structure. We choose banded LU decomposition for the solution of this system, since it is the most efficient method for such systems [55].

3.6 Algorithm

The algorithm we have used to solve the saturated groundwater flow equation using DG method in space and adaptive MOL in time is as follows:

1. based on input, construct the matrices and vectors which constitute the DG system and set the initial values
2. calculate the solution while stepping through time until reaching a time at which solution output is requested
3. output results
4. continue until the last solution sought is reached

3.7 Implementation Details

The temporal solver used [9] was developed in C++ with wrappers built around Fortran code. The DG method was implemented in C++. All numerical simulations were run in a single treaded manner on machines operating with RedHat Linux 7.2 with two 1.6 GHz AMD Athlon processors and 1 GB of RAM. All code was compiled with g++/gcc/g77 version 2.96.

Chapter 4

Results and Discussion

4.1 Introduction

In this chapter, we first present the test problems used to evaluate our solution method. This is followed by a description of the work and error measures. Lastly, we present and discuss the results of this evaluation.

4.2 Test Problems

We chose three problems to test our solution method, P1, P2 and P3. P1 is a simple smooth homogeneous problem, allowing for tests under ideal conditions; its solution is displayed in Figure 4.1. P2 is a problem with continuous but spatially variable conditions; its solution is shown in Figure 4.2. P3 is a difficult problem based on a highly variable discrete conductivity field; its solution is shown in Figure 4.3. The parameters used to describe these problems are displayed in Table 4.1. We solved P1 and P3 using both DG and BG, while only DG was run on P2.

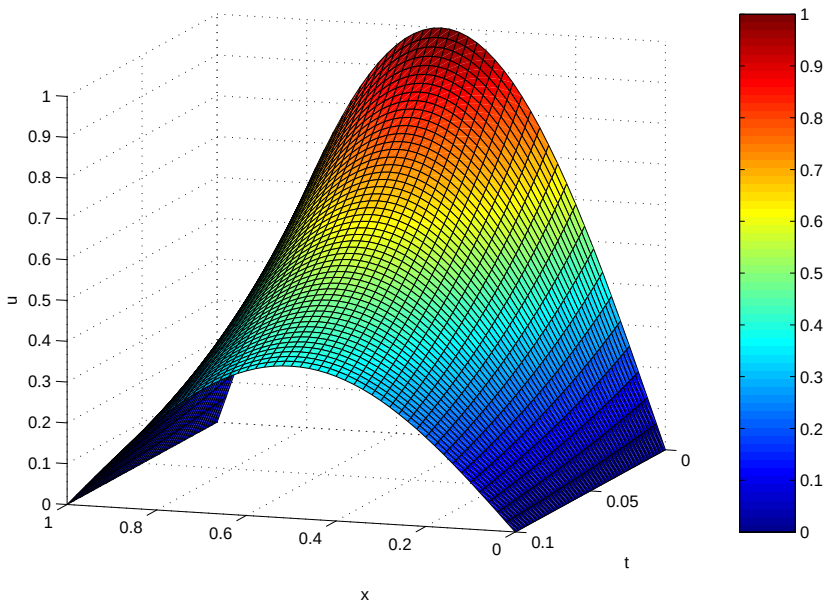

Figure 4.1: P1 solution over the domain.

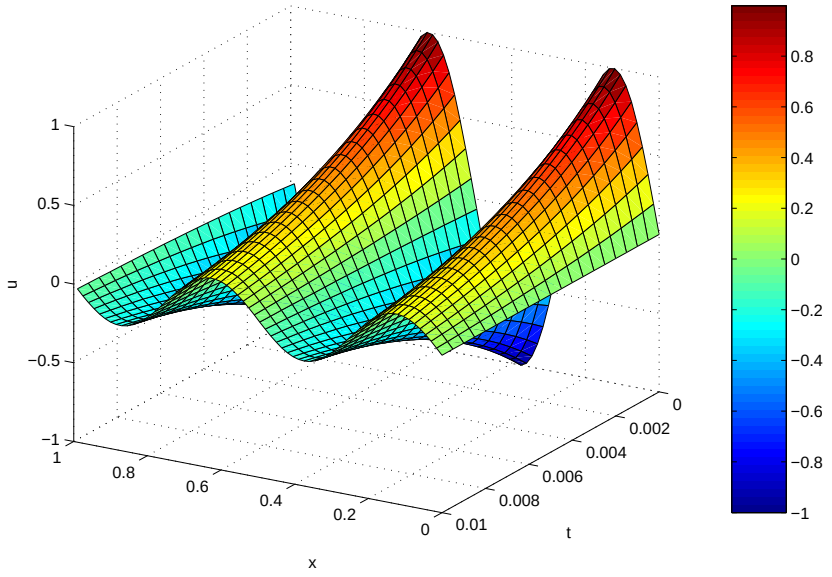

Figure 4.2: P2 solution over the domain.

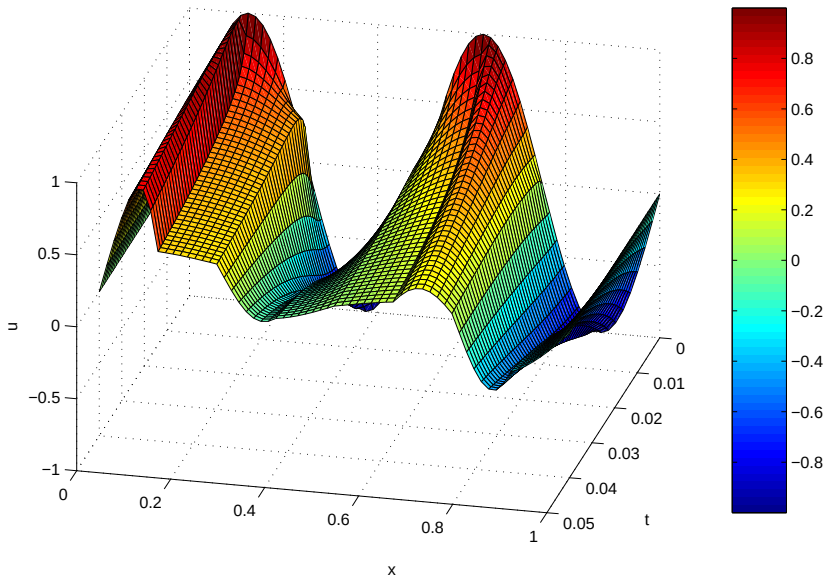

Figure 4.3: P3 solution over the domain.

Table 4.1: Test Problem Parameters.

Variable	P1	P2	P3
u_0	$sin(\pi x)$	$sin(4\pi x)$	$sin(4\pi x)$
u_{bl}	0	0	0
u_{br}	0	0	1
K	1	$2 + cos(4\pi x)$	see Table 4.2
S_s	1	$2 + sin(4\pi x)$	1
f	0	$16\pi^2 e^{-16\pi^2 t} sin(4\pi x)$	0
		$(2cos(4\pi x) - sin(4\pi x))$	
Ω	[0, 1]	[0, 1]	[0, 1]
T	0.1	0.01	0.04

4.3 Error and Work Measures

We used the L_2 norm to measure the error of our numerical solutions. The L_2 norms were calculated as

Table 4.2: Spatial distribution of K for P3.

x	K
(0,0.125)	0.001
(0.125,0.25)	1
(0.25,0.375)	0.01
(0.375,0.5)	0.5
(0.5,0.625)	0.0005
(0.625,0.75)	0.05
(0.75,0.875)	0.5
(0.875,1)	1

$$\epsilon_{L2} = \sqrt{\int_{\Omega} (u - \hat{u})^2 d\Omega} \qquad \text{at } t = T \tag{4.1}$$

where for P1 and P2 $\hat{u}$ is the analytic solution and for P3 $\hat{u}$ is a dense grid solution, since we lack an analytic solution. This dense grid solution was calculated with the parameters give in Table 4.3, where P_s is the spatial approximation order, P_t is the temporal approximation order, and as was defined in Section 3.3.1, N is the number of elements across the domain. N is lower for BG than for DG due to computational expense limitations. All the L_2 norms were calculated using Radau numerical quadrature integration.

We used CPU time t_{cpu} to measure computational work, using the ANSI C clock library. The CPU time reported here includes all the time required to run the code as described in Section 3.6, excluding time required for the output of results.

Table 4.3: P3 Dense Grid Solution Parameters

Variable	DG method	BG method
ϵ_a	10^{-14}	10^{-14}
ϵ_r	10^{-14}	10^{-14}
P_s	7	7
P_t	5	5
N	16384	4096

4.4 Numerical Comparisons

4.4.1 Preliminaries and Notation

For each of the test problems, we developed plots displaying the L_2 norm spatial h convergence rates and of work in comparison to error. In both forms of plots, each line represents a series of runs at the orders indicated in the legend. Each point on these lines represents a run at a different spatial grid spacing h. All the h values are also listed in the legend. Each line starts at the first h value listed, with each of the later points being a single progression down the list.

The h convergence rates plots consist of two sub-plots. The upper panel displays $log_{10}(\epsilon_{L2})$ as a function of $log_{10}(1/h)$, at a temporal order of five and various spatial orders, in the format described previously in this subsection. The slope of these lines is the h convergence rate achieved. The lower panel displays these convergence rates as a function of h.

The work versus error plots consist of four sub-plots, each displaying approximations of a different spatial order. These are plots of $log_{10}(\epsilon_{L2})$ as a function of $log_{10}(t_{cpu})$, for various temporal orders, in the format described earlier in this subsection.

The parameters used to make these plots are displayed in Table 4.4.

Table 4.4: Plot Parameters

variable	h convergence plots	work error plots
ϵ_a	10^{-14}	10^{-13}
ϵ_r	10^{-14}	10^{-13}
P_t	5*	2* - 5*

(*P_t values reported are the maximum value allowed under adaptive conditions)

We introduce the notion $DG_{P_tP_s}$, which represents a P_t temporal order and P_s spatial order approximation using the DG in space and adaptive higher-order FLCBDF in time. $BG_{P_tP_s}$ indicates the same for approximations using BG is space and FLCBDF in time. We will use the term efficiency to refer to a measure of reduction in the CPU time required to achieve the same level of error.

4.4.2 Findings

We were able to achieve expected L_2 norm spatial h convergence rates for P1 with both DG and BG, see Figure 4.4. With DG this means optimal convergence rates for odd spatial orders and suboptimal for even. BG holds to optimal rates at even and odd orders. As a result BG has higher convergence rates on even orders than does DG. These rates were found on grids as course as two and four elements over the domain and up to a spatial order of eight. For orders greater than eight on the same course grid, error became dominated by the temporal error near the ϵ_a and ϵ_r values of 10^{-14}, as the error failed to decrease with further spatial grid refinement. This lack of further error reduction near ϵ_a and ϵ_r, was found across a wide range of spatial orders, spatial grid spacings and temporal error tolerances.

With P1, we found significant improvements in accuracy and efficiency were gained by increasing temporal and spatial order, with both DG and BG, see Figure 4.5. For DG we found as much as seven orders of magnitude decrease in

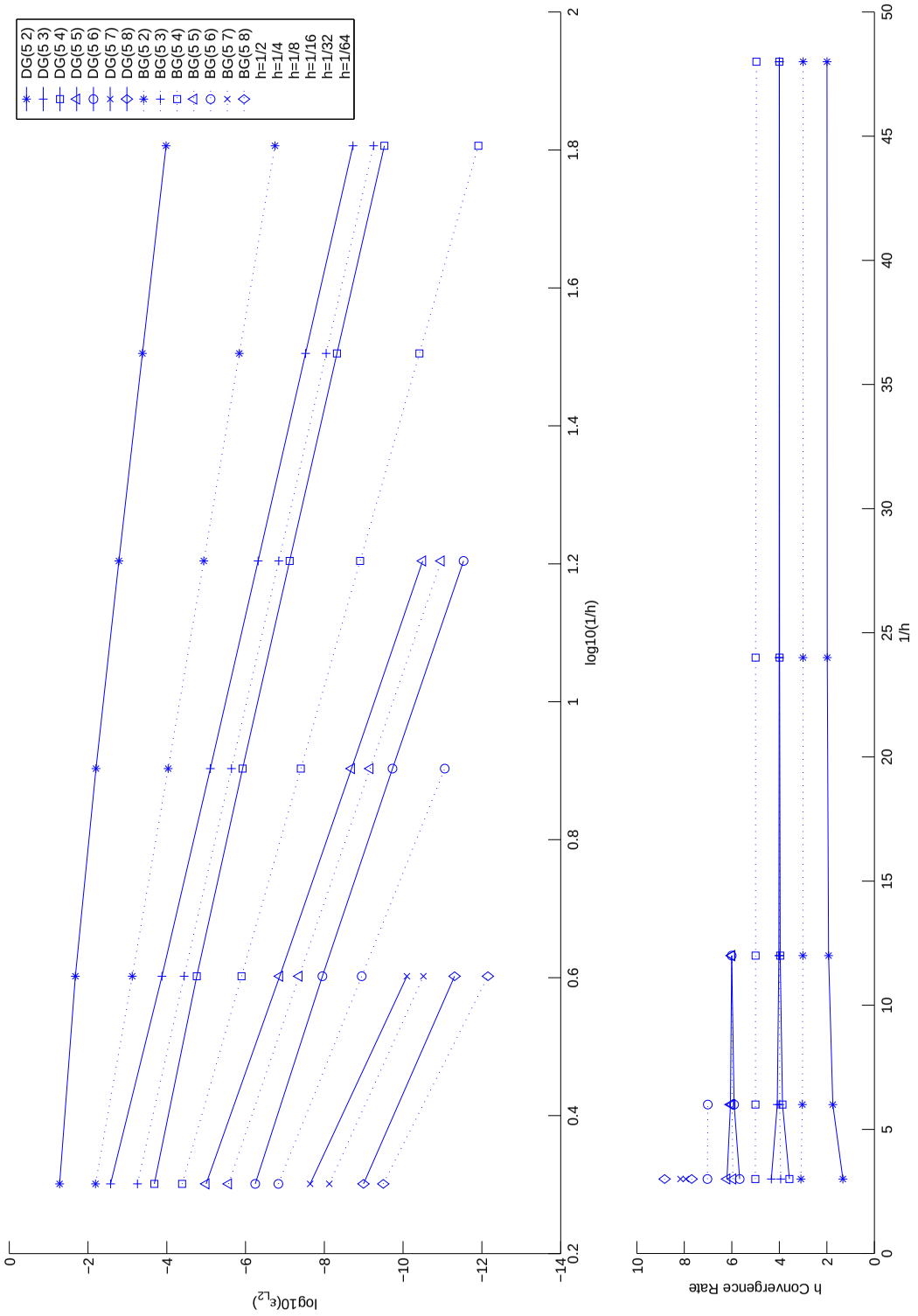

Figure 4.4: DG and BG h convergence rates for P1.

error and three orders of magnitude decrease in CPU time, when comparing DG_{22} with DG_{57}. Where this notation was defined in Section 4.4.1. While substantial improvements in these measures are also seen when both spatial and temporal orders are high in comparison to either of the possible low-order, high-order combinations. These incremental increases in efficiency with increases in order are somewhat diminished between higher-orders. BG's higher h convergence rate at the second spatial order, in comparison to DG, gives it an obvious advantage in the work error analysis as well. Aside from that order, across most spatial and temporal orders the results for DG and BG are comparable, while BG slightly out performs.

Continuing with the analysis of P1 in Figure 4.5, the CPU times for high-orders appear rather erratic. While we can only speculate at the source of this erratic nature, perhaps latency in data transfer with memory or hard disk, we can note the same behavior has been seen by others using this solver and that it has a low amplitude, which only appears to be of significance in comparison to the overall CPU time at short CPU times, on this log scale. With the coarser spatial grids, increases in the number of elements do not increase CPU time and in some cases, even result in a decrease in CPU time. This tread is due to a combination of the dominance of overall computational expense by non-scaling overhead operations and poor performance of the adaptive temporal integrater for approximations of low spatial order on course spatial grids, resulting in a greater number of time steps. The dominance of overall error by temporal error near the ϵ_a and ϵ_r values is the cause of the apparent lack of error reduction below these values with further increases in spatial order and spatial grid refinement. This temporal error is slightly greater at large CPU times, which correlate closely to the number of temporal integration steps for a given order coupling, as the error tolerances are applied at each step.

Beyond non-scaling overhead operations we expect that the computational expense would scale $\frac{1}{2}\eta P_s$ for DG and ηP_s for BG. As this is scaling rate for the

LU decomposition solution of the linear systems solved in these approximations. While the solution of these linear systems dominates our computational effort. Given the nearly constant h convergence rate we saw for P1 in Figure 4.4 and fixed spatial order associated with each line in Figure 4.5 we would expect the lines in the later plot to be linear. However, the lines in this plot are effected by the earlier explained lack in CPU time increase for increases in spatial grid refinement on coarse grids and the dominance temporal error on fine grids with high spatial order, which can both lead to an overall curvilinear appearance. For the lower temporal order couples the increase in temporal error with increases in the number of temporal steps explained earlier could also add to this curvilinear appearance. These treads are better illustrated with the less erratic CPU times of P2 in Figure 4.7.

The DG solutions of the more heterogeneous yet continuous P2 test problem has more error than that of P1 in comparing the same spatial order and grid densities, see Figure 4.6. This increase in error is more pronounced on the coarser grids, likely due to a lack of polynomial fit to larger period portions of sinusoidal curves. This reasoning could also be used to explain the non-ideal h convergence rates found on the coarser grids. The expected convergence rates are reached or approached on the denser grids.

In looking at Figure 4.7, we can see that DG solutions of P2 in comparison to those of P1 have larger errors across all spatial orders, temporal orders and grid densities. The improvements gained by increasing spatial and temporal order are slightly less than that found under the idea conditions of P1 but still substantial, with a seven order of magnitude decrease in error and a 2.5 order of magnitude decrease in CPU time, when comparing DG_{57} to DG_{22}. As with P1, the time savings and/or accuracy improvement of high-order, high-order couplings are significant in comparison to either of the high-order, low-order couplings. The lack of or even negative scaling of CPU time with spatial grid density on coarse grids as noted with P1 is apparent with P2. As is the temporal error dominance

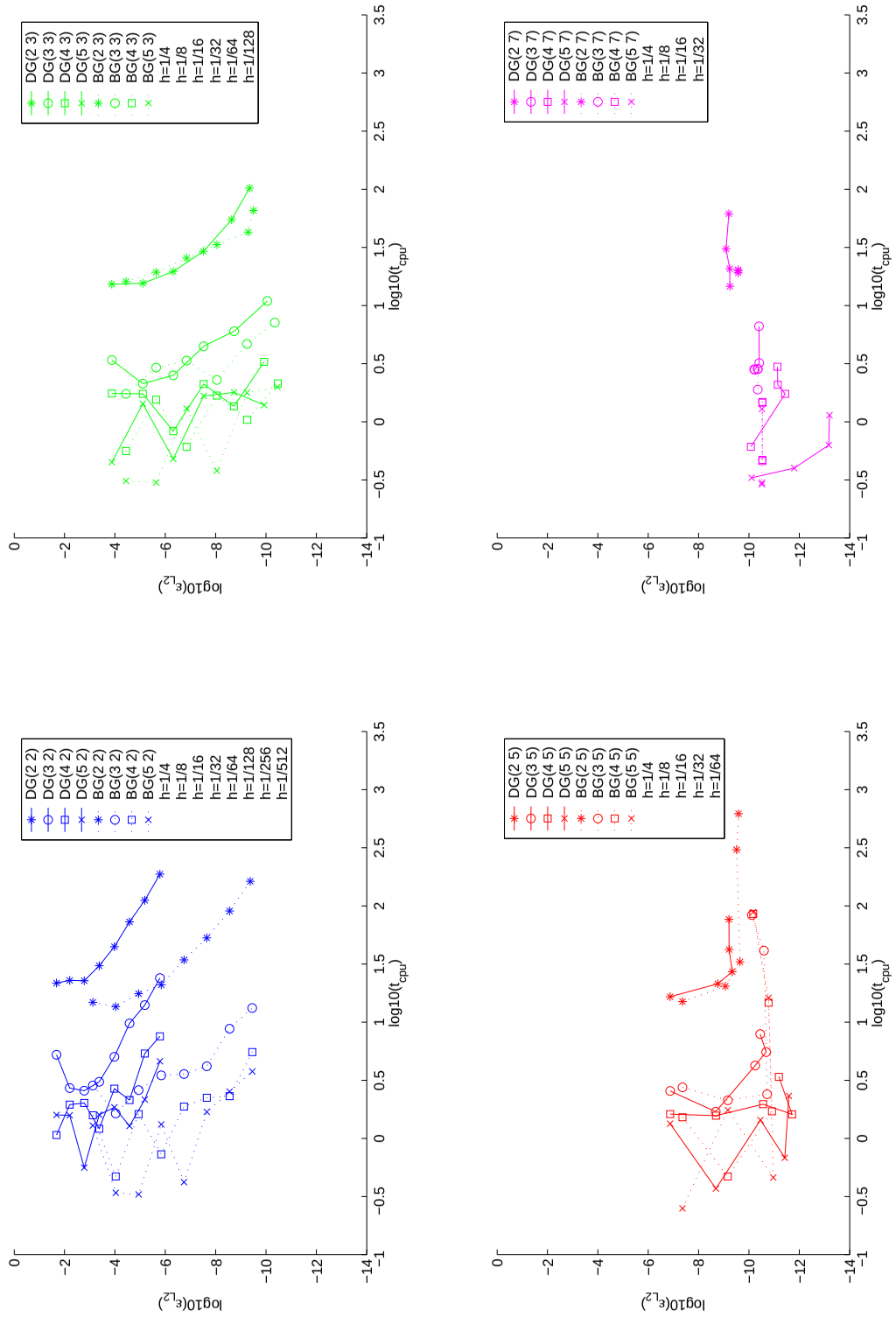

Figure 4.5: DG and BG work versus error for P1.

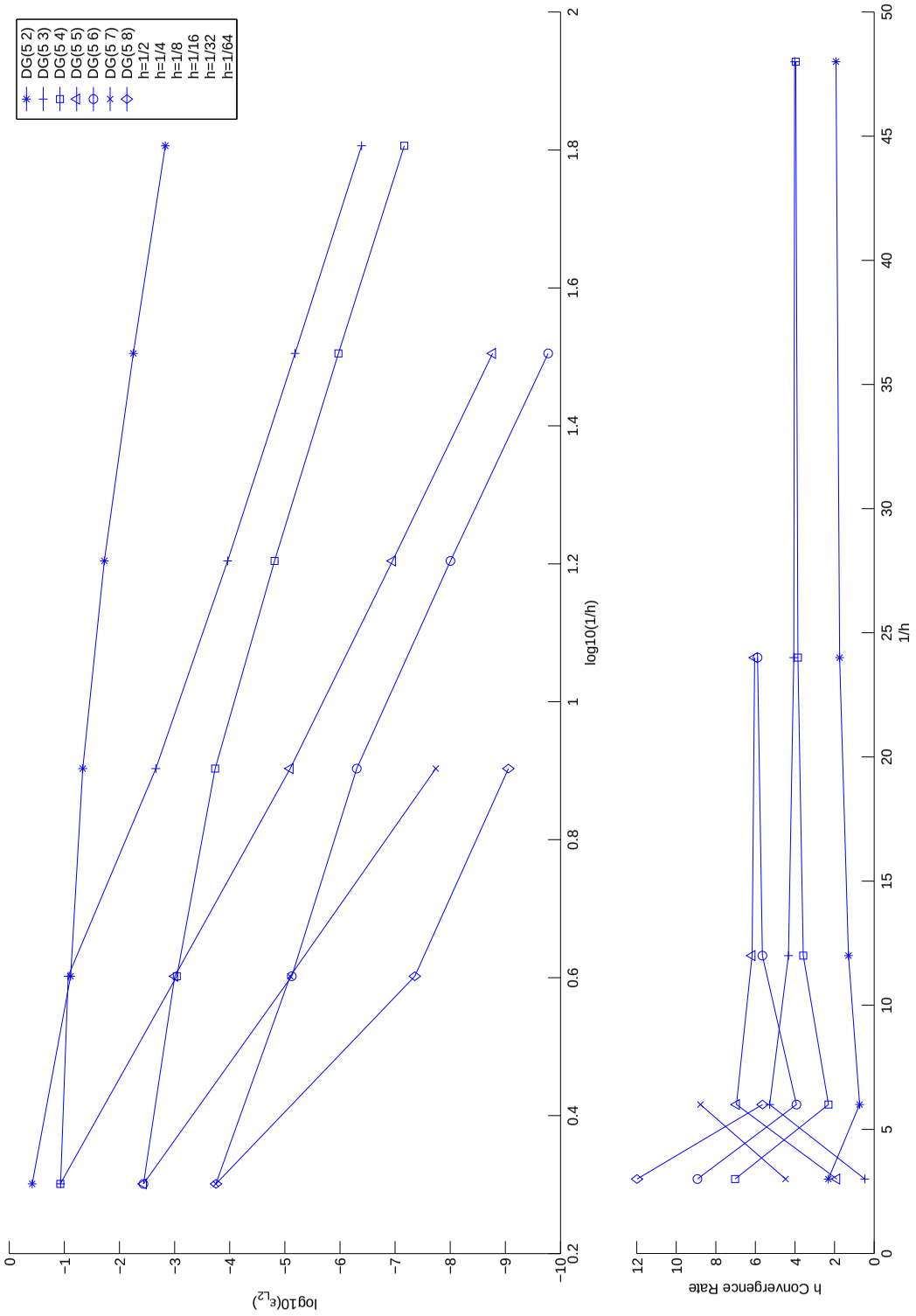

Figure 4.6: DG h convergence rates for P2.

for fine grids with higher order. These trends are more obvious with P2, since the CPU times for P2 are larger than the erratic CPU time fluctuations seen in P1.

It can be seen in Table 4.2 that the discrete conductivity field on which P3 is based varies by about 3.3 orders of magnitude. The error in the DG and BG solutions of P3 are significantly greater than those for the earlier test problems across all orders and grid densities, see Figure 4.8. Near ideal h convergence rates were achieved by DG and BG on grids of 256 elements and greater for most spatial orders. Ideal convergence rates were reached on grids as dense as 64 elements with DG for problems based on conductivity fields that varied by two orders of magnitude. A conductivity field varying by seven orders of magnitude holds a convergence rates of about 0.8 across all spatial orders for grids as dense as 256 with DG.

For P3, we find that the DG and BG solutions computed with high-order in both space and time show large savings in CPU time and reductions in error when compared to solutions with a low-order in either space or time or both. The DG solution of P3 yielded a four order of magnitude reduction in error and a two order of magnitude reduction in computation when comparing DG_{22} to DG_{57}. In the before mentioned case of a conductivity field that varied over seven orders of magnitude, we found a two order of magnitude decrease in CPU time at most levels of error, again comparing DG_{22} to DG_{57}.

In comparing DG to BG for solutions of P3, BG is slightly more efficient across most spatial and temporal orders. However, runs with a larger number of elements, across all spatial orders with equal convergence rates, BG requires less computational effort at lower temporal orders, but as temporal order increases this difference decreases and at a temporal order of five DG out performs BG. This trend is likely caused by a better temporal integration performance with DG, under these conditions. The lack of scaling of CPU time with grid density of coarse grids seen in P1 and P2 is apparent here as well. However, it does not

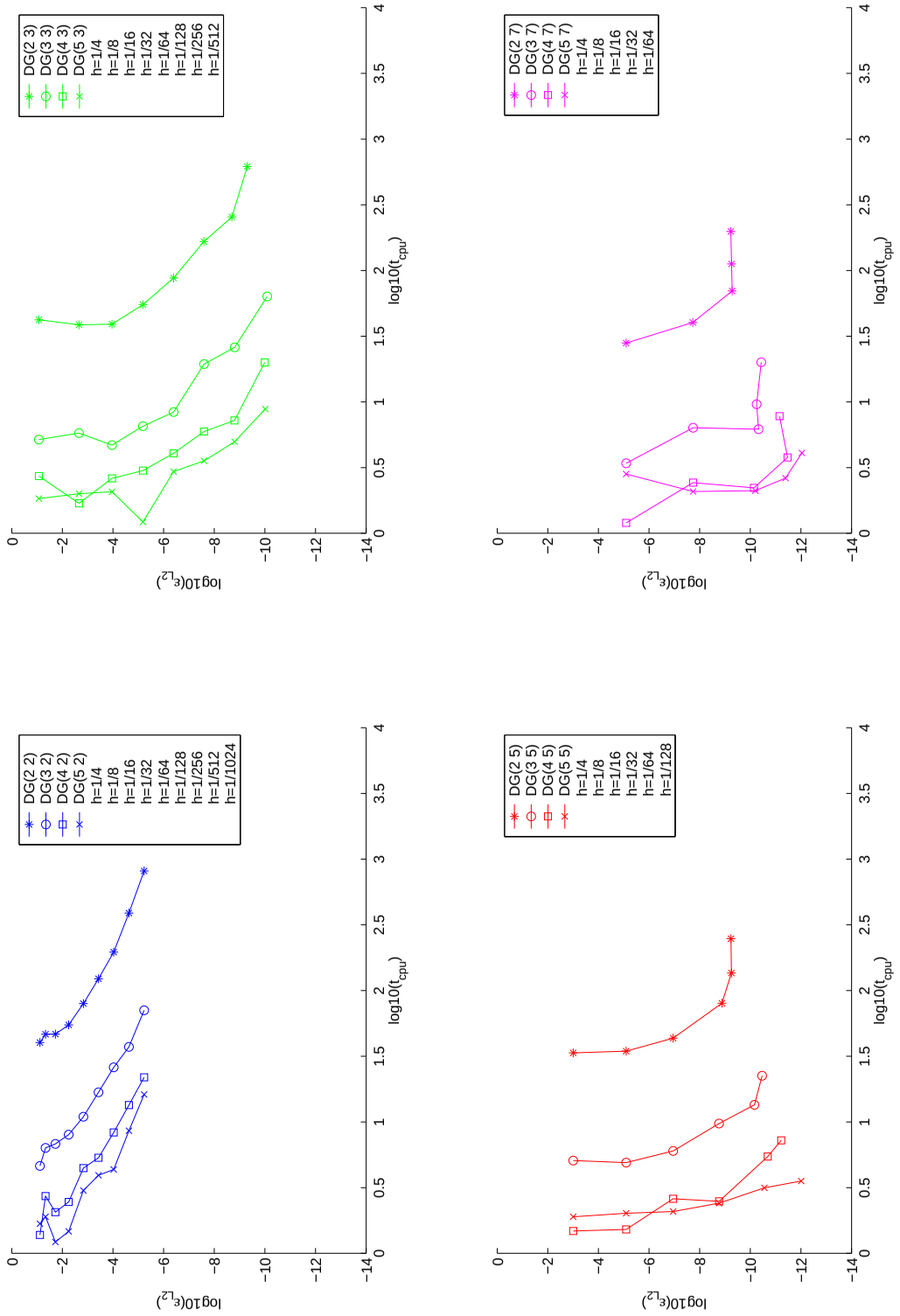

Figure 4.7: DG work versus error for P2.

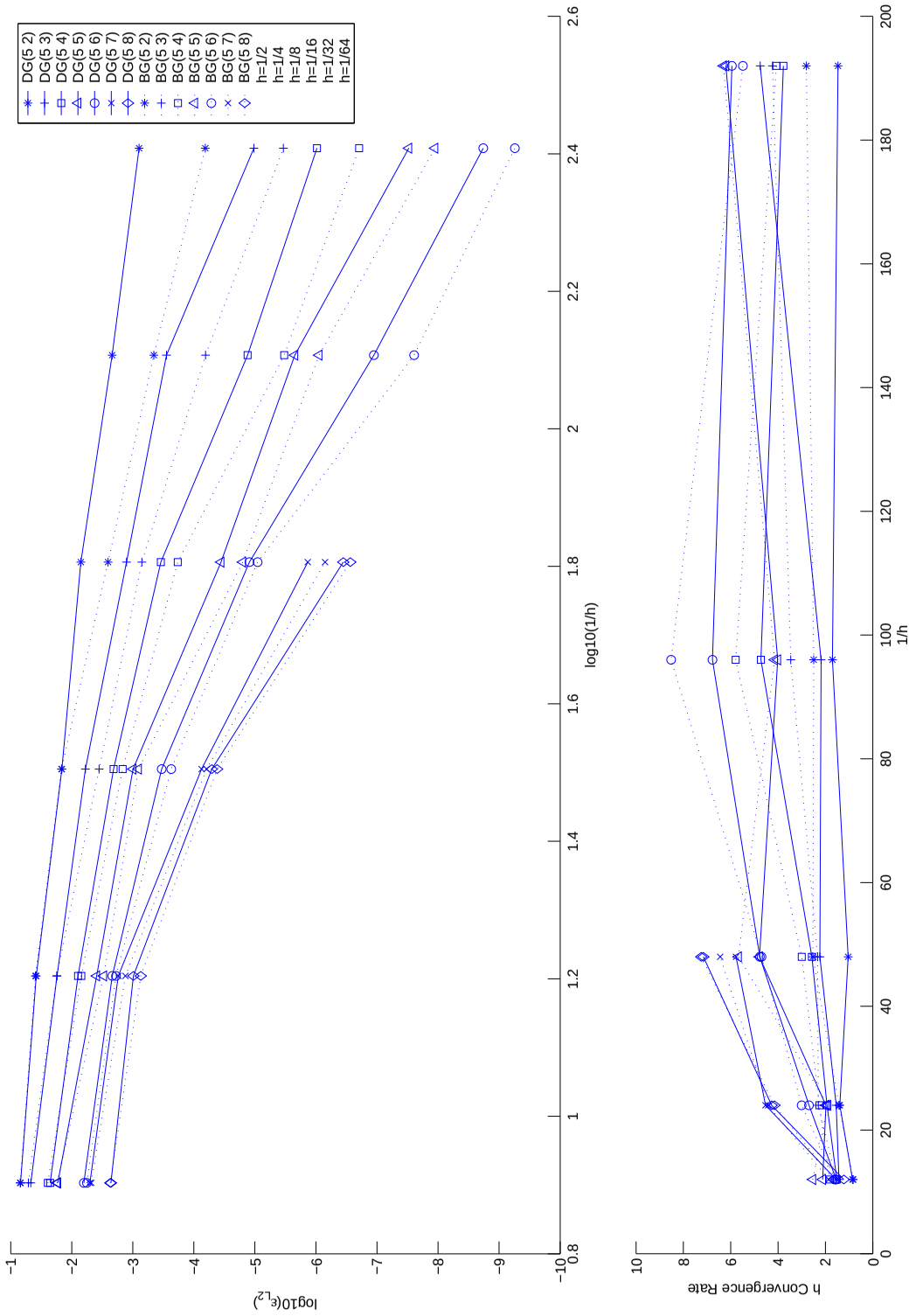

Figure 4.8: DG and BG h convergence rates for P3.

result in similar near vertical lines on this region, since the h convergence rates are low on these coarse grid. Near linear scaling is visible for high spatial orders.

With all of our test problems we have seen that large reductions in computation and error can be achieved by increasing temporal order when spatial order is low. We have also seen these improvements when increasing spatial order while temporal order is low. We found that error and computation can be substantially reduced below that found with these couplings by using high-orders in both time and space. Further more, we have demonstrated that when combined with adaptive higher-order MOL the mass conservative DG method is capable of high-order h convergence rates as with the non locally mass conservative BG and at a computational expense comparable to that of BG.

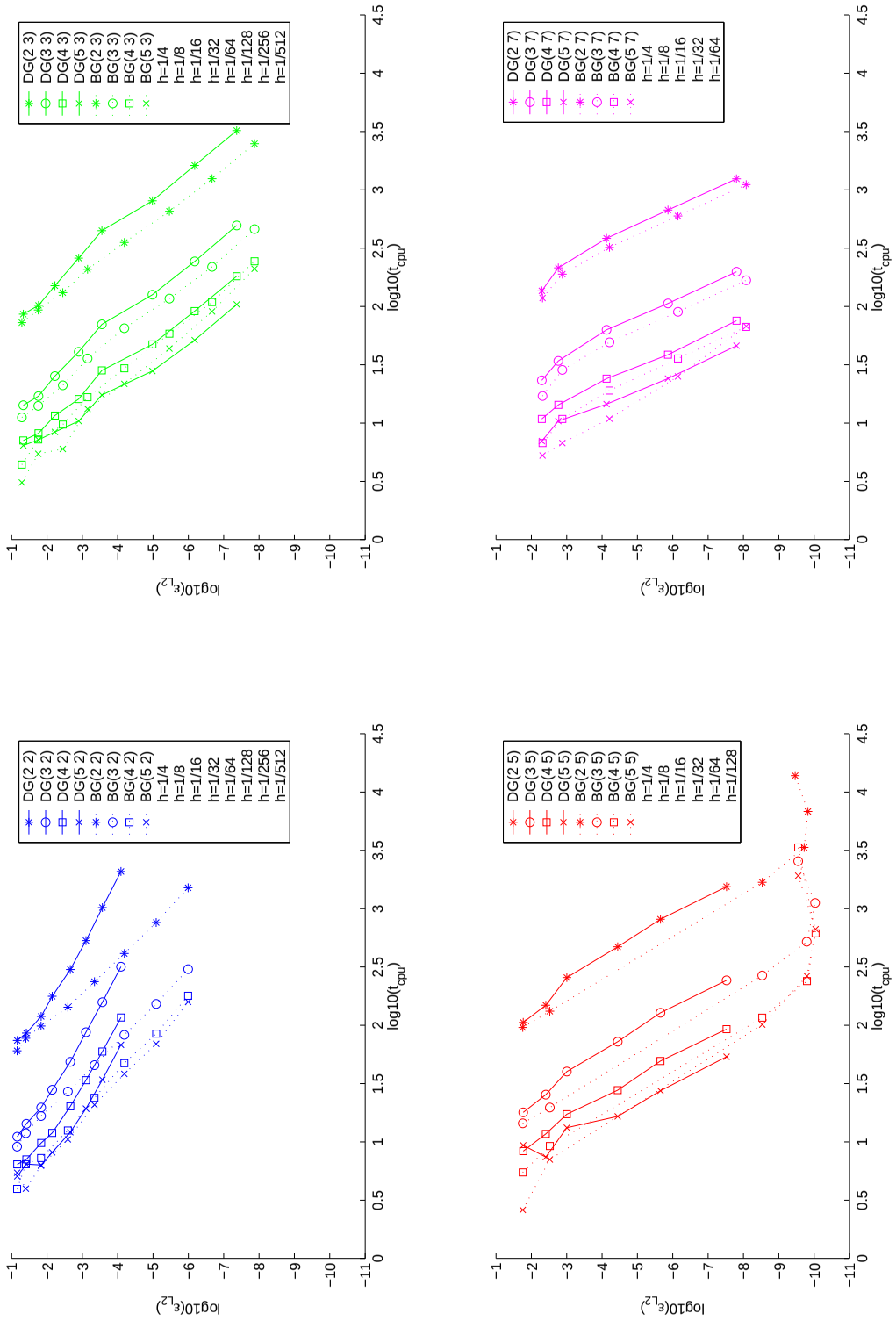

Figure 4.9: DG and BG work versus error for P3.

Chapter 5

Conclusions

- DG methods yield locally mass conservative approximations, can be easily extended to higher-order spatial approximations, and do not require the solution of additional unknowns for spatial derivatives as is required for mixed finite element methods.
- This is the first known extension of DG with a DAE MOL approach yielding higher-order approximations in space and time.
- Resulting approximations for a parabolic diffusion equation are robust and numerically efficient compared to standard low-order methods
- The methods explored may be extended to higher dimensions, fully adaptive approaches, and nonlinear problems.

REFERENCES

[1] P. Ackerer, A. Younes, and R. Mose. Modeling variable density flow and solute transport in porous medium I. numerical model and verification. *Transport in Porous Media*, 35:345–373, 1999.

[2] T. Arbogast, M. F. Wheeler, and I. Yotov. Mixed finite elements for elliptic problems with tensor coefficients as cell-centered finite differences. *SIAM Journal on Numerical Analysis*, 34(2):828–852, 1997.

[3] T. Arbogast, M. F. Wheeler, and N. Y. Zhang. A nonlinear mixed finite element method for a degenerate parabolic equation arising in flow in porous media. *SIAM Journal on Numerical Analysis*, 33(4):1669–1687, 1996.

[4] D. N. Arnold, F. Brezzi, B. Cockburn, and L. D. Marini. Unified analysis of discontinuous Galerkin methods for elliptic problems. *SIAM J. Numer. Anal.*, 39(5):1749–1779, 2001.

[5] I. Babuška, C. Baumann, and T. J. Oden. A discontinuous *hp* finite element method for diffusion problems: 1-D analysis. *Comput. Math. Appl.*, 37:103–122, 1999.

[6] P. Bastian and V. Reichenberger. Mulitgrid for higher order discontinuous Galerkin finite elements applied to groundwater flow.

[7] L. Bergamaschi and M. Putti. Mixed finite elements and newton-type linearizations for the solution of Richards' equation. *International journal for numerical methods in engineering*, 45:1025–1046, 1999.

[8] L. Bergamaschi and M. Putti. Mixed finite elements and newton-type linearizations for the solution of Richards' equation. *International journal for numerical methods in engineering*, 45:1025–1046, 1999.

[9] K. E. Brenan, S. L. Campbell, and L. R. Petzold. *The Numerical Solution of Initial Value Problems in Differential-Algebraic Equations*. Society for Industrial and Applied Mathematics, Philadelphia, PA, 1996.

[10] F. Brezzi and M. Fortin. *Mixed and Hybrid Finite Element Methods*. Springer-Verlag, New York, 1991.

[11] G. F. Carey and B. A. Finlayson. Orthogonal collocation on finite elements. *Chemical Engineering Science*, 30:587–596, 1975.

[12] M. A. Celia, E. T. Bouloutas, and R. L. Zarba. A general mass-conservative numerical solution for the unsaturated flow equation. *Water Resources Research*, 26(7):1483–1496, 1990.

[13] P. W. Chang and B. A. Finlayson. Orthogonal collocation method on finite elements for elliptic equations. *Advances in Computer Methods for Partial Differential Equations — II*, pages 79–86, 1977.

[14] G. Chavent and J. E. Roberts. A unified physical presentation of mixed, mixed-hybrid finite elements and standard finite difference approximations for the determination of velocities in waterflow problems. *Advances in Water Resources*, 14(6):329–348, 1991.

[15] Z. Chen and R. E. Ewing. From single-phase to compositional flow: applicability of mixed finite elements. *Transport in Porous Media*, 27:225–242, 1997.

[16] Z. Chen and R. E. Ewing. Fully discrete finite element analysis of multiphase flow in groundwater hydrology. *SIAM Journal on Numerical Analysis*, 34 (6):2228–2253, 1997.

[17] L. M. Chounet, D. Hilhorst, C. Jouron, Y. Kelanemer, and P. Nicolas. Simulation of water flow and heat transfer in soils by means of a mixed finite element method. *Advances in Water Resources*, 22(5):445–460, 1999.

[18] Bernardo Cockburn and Chi-Wang Shu. The Runge-Kutta local projection P^1-discontinuous Galerkin method for scalar conservation laws. *RAIRO Modél. Math. Anal.Numér.*, 25:337–361, 1991.

[19] Bernardo Cockburn and Chi-Wang Shu. The local discontinuous Galerkin method for time-dependent convection-diffusion systems. *SIAM J. Numer. Anal.*, 35:2440–2463, 1998.

[20] C. Cordes and K. Kinzelbach. Continuous groundwater velocity field and path lines in linear, bilinear, and trilinear finite elements. *Water Resources Research*, 28(11):2903–2911, 1992.

[21] J. C. Crittenden and W. J. Weber, Jr. Model for design of multicomponent adsorption systems. *Journal of Environmental Engineering, ASCE*, 104(EE6):1175–1195, 1978.

[22] J. C. Crittenden and W. J. Weber, Jr. Predictive model for design of fixed bed adsorbers: Parameter estimation and model development. *Journal of Environmental Engineering, ASCE*, 104(EE2):185–197, 1978.

[23] J. C. Crittenden and W. J. Weber, Jr. Predictive model for design of fixed-bed adsorbers: Single-component model verification. *Journal of Environmental Engineering, ASCE*, 104(EE3):433–443, 1978.

[24] J. C. Crittenden, B. W. Wong, W. E. Thacker, V. L. Snoeyink, and R. L. Hinrichs. Mathematical model of sequential loading in fixed-bed adsorbers. *Journal of the Water Pollution Control Federation*, 52(11):2780–2795, 1980.

[25] H. Darcy. *Les Fontaines Publiques de la Ville de Dijon*. Dalmont, Paris, 1856.

[26] C. N. Dawson. Conservative, shock-capturing transport methods with non-conservative velocity approximations. Technical Report TICAM 99-28, University of Texas, Austin, TX, 1999.

[27] C. N. Dawson, M. F. Wheeler, and C. S. Woodward. A two-grid finite difference scheme for nonlinear parabolic equations. *SIAM Journal on Numerical Analysis*, 35(2):435–452, 1998.

[28] L.J. Durlofsky. Accuracy of mixed and control volume finite element approximations to Darcy velocity and related quantities. *Water Resources Research*, 30(4):965–973, 1994.

[29] L.J. Durlofsky. Accuracy of mixed and control volume finite element approximations to Darcy velocity and related quantities. *Water Resources Research*, 30(4):965–973, 1994.

[30] M. W. Farthing, C. E. Kees, and C. T. Miller. Mixed finite element methods and higher order temporal approximations. In *American Geophysical Union Spring Meeting*, volume 81(19) of *EOS Transactions*, page S233. American Geophysical Union, 2000.

[31] M. W. Farthing, C. E. Kees, and C. T. Miller. Mixed finite element methods and higher-order temporal approximations. *Advances in Water Resources*, 25(1):85–101, 2002.

[32] M. W. Farthing, C. E. Kees, and C. T. Miller. Mixed finite element methods and higher order temporal approximations for variably saturated groundwater flow. *in review*, 2002.

[33] B. Finlayson. *The Method of Weighted Residuals and Variational Principles*. Academic Press, New York, NY, 1972.

[34] B. A. Finlayson. Packed bed reactor analysis by orthogonal collocation. *Chemical Engineering Science*, 26:1081–1091, 1971.

[35] P.A. Forsyth, Y.-S. Wu, and K. Pruess. Robust numerical methods for saturated-unsaturated flow with dry initial conditions in heterogeneous media. *Advances in Water Resources*, 18:25–38, 1995.

[36] R. A. Freeze and J. A. Cherry. *Groundwater*. Prentice-Hall, Inc., Englewood Cliffs, NJ, 1979.

[37] C. W. Gear. The automatic integration of stiff ordinary differential equations. .

[38] C. W. Gear. Numerical integration of ordinary differential equations. .

[39] C. W. Gear. *Numerical Initial Value Problems in Ordinary Differential Equations*. Prentice-Hall, Englewood Cliffs, NJ, 1971.

[40] C. W. Gear. *Numerical Initial Value Problems in Ordinary Differential Equations*. Prentice-Hall, Englewood Cliffs, NJ, 1971.

[41] V. Girault, B. Rivière, and M. F. Wheeler. A discontinuous Galerkin method with non-overlapping domain decomposition for the Stokes and Navier-Stokes problems. Report 02-08, TICAM, Austin, 2002.

[42] G. Golub and C. F. van Loan. *Matrix Computations*. The Johns Hopkins University Press, Baltimore and London, 1989.

[43] R. Huber and R. Helmig. Multiphase flow in heterogeneous porous media: a classical finite element method versus an implicit pressure-explicit saturation-based mixed finite element-finite volume approach. *International journal for numerical methods in fluids*, 29:899–920, 1999.

[44] R. Huber and R. Helmig. Multiphase flow in heterogeneous porous media: a classical finite element method versus an implicit pressure-explicit saturation-based mixed finite element-finite volume approach. *International journal for numerical methods in fluids*, 29:899–920, 1999.

[45] A.I. James and W.D. Graham. Numerical approximation of head and flux covariances in three dimensions using mixed finite elements. *Advances in Water Resources*, 22(7):729–740, 1999.

[46] Douglas J. Jr. The mathematical foundations of the finite element method with application to partial differential equations. *Academic Press, New York*, 1972.

[47] S.-H. Ju and K.-J. S. Kung. Mass types, element orders and solution schemes for the Richards equation. *Computers and Geosciences*, 23(2):175–187, 1997.

[48] D. Kavetski, P. Binning, and S. W. Sloan. Adaptive time stepping and error control in a mass conservative numerical solution of the mixed form of richards equation. *Advances in Water Resources*, 24(6):595–605, 2001.

[49] D. Kavetski, P. Binning, and S.W. Sloan. Adaptive time stepping and error control in a mass conservative numerical solution of the mixed form of Richards' equation. *Advances in Water Resources*, 24:595–605, 2001.

[50] C. E. Kees and C. T. Miller. C++ implementations of numerical methods for solving differential-algebraic equations: Design and optimization considerations. *Association for Computing Machinery, Transactions on Mathematical Software*, 25(4):377–403, 1999.

[51] C. E. Kees and C. T. Miller. Higher order time integration methods for two-phase flow. *Advances in Water Resources*, 25(2):159–177, 2002.

[52] C.E. Kees and C.T. Miller. Higher order time integration methods for two-phase flow. *Advances in Water Resources*, 25(2):159–177, 2002.

[53] C. T. Kelley, C. T. Miller, and M. D. Tocci. Termination of Newton/chord iterations and the method of lines. *SIAM Journal on Scientific Computing*, 19:280–290, 1998.

[54] F. Lehmann and Ph. Ackerer. Comparison of iterative methods for improved solutions of the fluid flow equation in partially saturated porous media. *Transport in Porous Media*, 31(3):275–292, 1998.

[55] G. Meurant. *Computer Solution of Large Linear Systems*. North-Holland, Amsterdam, 1999.

[56] C.T. Miller, M.W. Farthing, C.E. Kees, and C.T. Kelley. Higher order, locally conservative temporal integration methods for modeling multiphase flow in porous media. In *XIV International Conference on Computational Methods in Water Resources*, Delft, The Netherlands, 2002.

[57] R. Mosé, P. Siegel, and P. Ackerer. Application of the mixed hybrid finite element approximation in a groundwater flow model: Luxury or necessity? *Water Resources Research*, 30(11):3001–3012, 1994.

[58] T. J. Oden, I. Babuška, and C. Baumann. A discontinuous *hp* finite element method for diffusion problems. *J. Comput. Phys.*, 146:491–519, 1998.

[59] T. J. Oden and C. Baumann. A conservative DGM for convection-diffusion and Navier-Stokes problems. In B. Cockburn, G. E. Karniadakis, and C. Shu, editors, *Discontinuous Galerkin Methods*, pages 179–196, 2000.

[60] J. A. Pedit and C. T. Miller. The advantage of high-order basis functions for modeling multicomponent sorption kinetics. In M. A. Celia, L. A. Ferrand, C. A. Brebbia, W. G. Gray, and G. F. Pinder, editors, *Proceedings of the VII International Conference, Computational Methods in Water Resources*, volume Computational Methods in Water Resources, Vol. 2: Numerical Methods for Transport and Hydrologic Processes, pages 293–298, Southampton, UK, 1988. Computational Mechanics Publications.

[61] B. Rivière and M. F. Wheeler. A discontinuous Galerkin method applied

to nonlinear parabolic equations. In B. Cockburn, G. E. Karniadakis, and C. Shu, editors, *Discontinuous Galerkin Methods*, pages 231–244, 2000.

[62] B. Rivière, M. F. Wheeler, and K. Banaś. Part II. discontinuous Galerkin method applied to single phase flow in porous media. *Computational Geosciences*, 4:337–349, 2000.

[63] J. Simunek, T. Vogel, and M. Th. van Genuchten. The SWMS_2D code for simulating water flow and solute transport in two-dimensional variably saturated media. Technical Report Research Report 132, U. S. Salinity Laboratory, Agriculatural Research Service, U. S. Department of Agriculture, Riverside, CA, 1994.

[64] M. D. Tocci, C. T. Kelley, and C. T. Miller. Accurate and economical solution of the pressure-head form of Richards' equation by the method of lines. *Advances in Water Resources*, 20(1):1–14, 1997.

[65] M. D. Tocci, C. T. Kelley, C. T. Miller, and C. E. Kees. Inexact Newton methods and the method of lines for solving Richards' equation in two space dimensions. *Computational Geosciences*, 2(4):291–309, 1999.

[66] J. V. Villadsen and W. E. Stewart. Solution of boundary-value problems by orthogonal collocation. *Chemical Engineering Science*, 22:1483–1501, 1967.

[67] W. J. Weber, Jr. and J. C. Crittendon. Madam i — a numeric design for method for adsorption systems. *Journal of the Water Pollution Control Federation*, 47(5):924–940, 1975.

[68] M. F. Wheeler. An elliptic collocation-finite element method with interior penalties.

[69] Y.-S. Wu and P.A. Forsyth. On the selection of primary variables in numerical formulation for modeling multiphase flow in porous media. *Journal of Contaminant Hydrology*, 48:277–304, 2001.

[70] A. Younes, R. Mosé, P. Ackerer, and G. Chavent. A new formulation of the mixed finite element method for solving elliptic and parabolic PDE with triangular elements. *J. Comp. Phys.*, 149:148–167, 1999.

[71] A. Younes, R. Mosé, P. Ackerer, and G. Chavent. A new formulation of the mixed finite element method for solving elliptic and parabolic PDE with triangular elements. *J. Comp. Phys.*, 149:148–167, 1999.